Computation of Turbomachinery Flow by a Convective-Upwind-Split-Pressure (CUSP) Scheme

*Feng Liu**
Department of Mechanical and Aerospace Engineering
University of California, Irvine, CA

Ian K. Jennions†
ABB Power Generation, Baden, Switzerland

Antony Jameson‡
Department of Aeronautics and Astronautics
Stanford University, Stanford, CA

Abstract

An artificial dissipation scheme using the concepts of SLIP and CUSP is implemented on top of a baseline three-dimensional turbomachinery flow code. The original baseline code uses a finite-volume method for the Navier-Stokes equations with classical Jameson-Schmidt-Turkel(JST) scalar dissipation scheme. This paper focuses on the comparison of the performance of the CUSP scheme with the original JST scheme for turbomachinery flow calculations. The results show that the CUSP scheme is more reliable than the JST scheme and is capable of providing accurate loss predictions on relatively coarse grids.

1 Introduction

With the increased power of computers and improved numerical methods, solution of the Navier-Stokes equations has become a common place for aerodynamic design of compressors and turbines used in both aero-propulsion and ground-based gas turbines. Due to its simplicity, computational efficiency and robustness, the finite-volume method using adaptive scalar artificial dissipation originally proposed by Jameson Schmidt and Turkel[1] (herein called the JST scheme) has been used in many production codes for turbomachinery calculations, including one used at ABB Power Generation[2, 10]. As CFD is used more in the design process, the designer also demands more on the accuracy, efficiency and robustness of a CFD code. The simple JST scheme has been blamed on by some researchers for inaccuracies in resolving boundary layers and sharp shock fronts. While more elaborate TVD, flux-splitting, and flux-difference splitting schemes have been developed and cited for their improved accuracy, they usually tend to exhibit less computational efficiency and robustness. In addition, the somewhat increased complexity in coding of these schemes also have limited their adoption in production codes used in industry.

Recently, Jameson proposed new artificial dissipation methods based on Symmetric LImited Positive (SLIP) schemes and a simple Convective Upwind Split Pressure (CUSP) scheme for the Euler equations[4, 5]. These new schemes have been found to provide comparable high resolution for shock waves[4, 5] and viscous boundary layers[6, 7] as by the conventional TVD, flux-splitting, and flux-difference splitting schemes while at the same time retaining the simplicity, computational efficiency and robustness of the original JST scheme.

In this work, we implement a CUSP scheme based on [4, 5] in a three-dimensional turbomachinery flow code. The baseline code uses the original JST scheme for solving the Navier-Stokes equations with the Baldwin-Lomax algebraic turbulence model (see Liu and Jameson[3]). Computations using the new scheme were done for a number of practical test cases at ABB Power Generation. The new code has been found to provide better accuracy and robustness with the same computational efficiency. In this paper, however, we will focus on the perfomance of the CUSP scheme on a supersonic wedge cascade and a three-dimensional subsonic turbine vane. In the following two sections, we will first outline the original baseline code and then present the CUSP scheme used for our turbomachinery flow calculations. Section 4 presents the comparison of the the computational results with the original JST scheme.

*Associate Professor, Member AIAA
†Manager, Member AIAA
‡Professor, Fellow AIAA

2 The Baseline Code with JST Artificial Dissipation

The baseline code, called turbo90, uses a finite-volume method for the Naver-Stokes equation[3]. The JST scalar artificial dissipation is implemented with a multi-stage Runge-Kutta time stepping scheme to drive the computation to a steady state. Local time-stepping, residual smoothing, and multi-grid are used to accelerate convergence.

We first outline the basic JST dissipation scheme of the baseline code for convenient discussion of the new CUSP scheme in the next section.

Since implementation of a particular artificial dissipation model in three dimensions is achieved here through the application of a one-dimensional model in each of the three grid directions, we will illustrate the schemes in one dimension only. A 1-D conservation law can be written as

$$\frac{\partial v}{\partial t} + \frac{\partial f(v)}{\partial x} = 0 \tag{1}$$

With a finite volume spatial discretization, the above equation becomes

$$\frac{\partial v}{\partial t} + h_{j+\frac{1}{2}} - h_{j-\frac{1}{2}} = 0 \tag{2}$$

where

$$h_{j+\frac{1}{2}} = \frac{1}{2}(f_{j+\frac{1}{2}} + f_{j-\frac{1}{2}}) - d_{j+\frac{1}{2}} \tag{3}$$

$d_{j+\frac{1}{2}}$ is the dissipation flux.

Within the above framework, schemes of various kinds are distinguished by the formulation of this dissipation flux term. Upwind biasing can be essentially achieved by the appropriate choice of $d_{j+\frac{1}{2}}$.

The classical Jameson-Schmidt-Turkel (JST) scheme[1]. uses blended 1st and 3rd differences to form the artificial dissipation fluxes needed for stability and capturing shock waves. A pressure based switch is used to turn on the 1st differences near shock waves. This is done by setting

$$\begin{aligned} d_{j+\frac{1}{2}} &= \epsilon^{(2)}_{j+\frac{1}{2}} \Delta v_{j+\frac{1}{2}} \\ &\quad -\epsilon^{(4)}_{j+\frac{1}{2}} (\Delta v_{j+\frac{3}{2}} - 2\Delta v_{j+\frac{1}{2}} + \Delta v_{j-\frac{1}{2}}) \end{aligned} \tag{4}$$

$$Q_j = \left| \frac{p_{j+1} - 2p_j + p_{j-1}}{p_{j+1} + 2p_j + p_{j-1}} \right| \tag{5}$$

$$S_{j+\frac{1}{2}} = max(Q_j, Q_{j+1})$$

$$\epsilon^{(2)}_{j+\frac{1}{2}} = k_2 min(1, \beta_1 S_{j+\frac{1}{2}}) \alpha_{j+\frac{1}{2}} \tag{6}$$

$$\epsilon^{(4)}_{j+\frac{1}{2}} = max(0, k_4 \alpha_{j+\frac{1}{2}} - \beta_2 \epsilon^{(2)}_{j+\frac{1}{2}}) \tag{7}$$

$$\beta_1 = 2 \sim 4, \quad \beta_2 = 1$$

$$k_2 = O(1), \quad k_4 = 1 \sim \frac{1}{32}$$

where $\alpha_{j+\frac{1}{2}}$ is an appropriate dissipation coefficient that is chosen to reduce the scheme into an upwinding one near a shock when $k_2 = 1$ for a 1-D scalar conservation law. This is achieved by setting

$$\alpha_{j+\frac{1}{2}} = \frac{1}{2} |a_{j+\frac{1}{2}}| \tag{8}$$

where

$$a_{j+\frac{1}{2}} = \begin{cases} \frac{f_{j+1} - f_j}{u_{j+1} - u_j} & \text{if } u_{j+1} \neq u_j \\ \frac{\partial f}{\partial u}|_j & \text{if } u_{j+1} = u_j \end{cases} \tag{9}$$

which is essentially the eigenvalue of the Jacobian of f.

For systems of conservation laws, f is a vector and in principle one needs to carry out a characteristic decomposition of the system of equations and apply the above to each component of the decomposed equations. A simplified and more economical way is to use the maximum eigenvalue of $A = \frac{\partial f}{\partial u}$ in equation (8) for all the equations of the system. Thus, in the original JST scheme $a_{j+\frac{1}{2}}$ is set to be

$$a_{j+\frac{1}{2}} = max(|u + c|, |u - c|, |u|) = |u| + |c|$$

In the baseline turbomachinery code, the above artificial dissipation scheme is used.

3 The New Scheme Based on SLIP and CUSP

As can be seen in the above discussions, the design of a dissipation scheme consists of two parts. The first part is to construct a high resolution non-oscillatory scheme for a scalar conservation law. The second part is to construct a numerical flux for a system of equations with different wave directions and speeds.

In the classical JST scheme the first part is done through the use of blended first and third differences with a pressure switch to sense the presence of shock waves where first order upwinding is needed. The second part is done by using a scalar diffusion parameter to reduce coding complexity and computational time.

Other more sophisticated schemes for both the first part and the second part can be constructed and various combinations of them can be used. Recently, Jameson discussed the construction of ELED (Essentially Local Extrema Diminishing) and CUSP schemes in [4, 5]. ELED is a principle for constructing high resolution schemes, and CUSP is a flux splitting scheme that combines simplicity, efficiency and high resolution of shocks without using characteristic splitting.

3.1 The SLIP Scheme

A systematic way of obtaining ELED schemes is to use the concept of flux limiting. In particular, a class of limiting schemes called Symmetric LImited Positive (SLIP) schemes can be used(see [4, 5]). In this class of schemes, an anti-diffusion term is added to the 1st order numerical dissipation scheme to achieve 2nd order accuracy.

$$d_{j+\frac{1}{2}} = \alpha_{j+\frac{1}{2}}[\Delta v_{j+\frac{1}{2}} - L(\Delta v_{j+\frac{3}{2}}, \Delta v_{j-\frac{1}{2}})] \quad (10)$$

where L is a limited average of $\Delta v_{j+\frac{3}{2}}$ and $\Delta v_{j-\frac{1}{2}}$. L is designed to achieve the arithmetic mean operator to approach 2nd order accuracy in smooth regions while approaching zero at extrema to obtain an non-oscillatory scheme.

Reference [4] proves that if L satisfies the following condition the above flux limited scheme for a scalar conservation law is LED.

P1: $L(u,v) = L(v,u)$
P2: $L(\alpha u, \alpha v) = \alpha L(v,u)$
P3: $L(u,u) = u$
P4: $L(u,v) = 0$, if u and v have opposite signs, otherwise $L(u,v)$ has the same sign.

LED schemes can also be made ELED by modifying the limiter L. In particular, the following limiter is used in the current implementation.

$$L(u,v) = \frac{1}{2}D(u,v)(u+v) \quad (11)$$

where

$$D(u,v) = 1 - \left|\frac{u-v}{|u|+|v|+\epsilon\Delta x^r}\right|^q \quad (12)$$

with $r = \frac{3}{2}$, and $q = 3$. $\Delta x = \frac{1}{JM}$, $\epsilon = AVA * v_{ref}$, where

$$v_{ref} = \begin{cases} \rho_{ref} & \text{for the mass equation} \\ \rho_{ref}V_{ref} & \text{for the momentum equations} \\ \rho_{ref}H_{ref} & \text{for the energy equation} \end{cases} \quad (13)$$

The reference point is taken to be the sonic point for given stagnation pressure p_0 and stagnation temperature T_0.

$$p_{ref} = \frac{p_0}{(1+\frac{\gamma-1}{2}M^2_{sonic})^{\frac{\gamma}{\gamma-1}}} = p_0(\frac{2}{\gamma+1})^{\frac{\gamma}{\gamma-1}}$$

$$T_{ref} = T_0(\frac{2}{\gamma+1})$$

$$\rho_{ref} = \frac{p_{ref}}{RT_{ref}}$$

$$V_{ref} = \sqrt{\gamma\frac{p_{ref}}{\rho_{ref}}}$$

$$H_{ref} = C_pT_0$$

3.2 The CUSP Splitting

The schemes discussed in Section 3.1 tell us how to construct difference terms for scalar conservation laws, where $\alpha_{j+\frac{1}{2}}$ in Equation (10) is half of the wave speed. For systems of equations, strictly speaking, we need to decompose the original conservation laws into 5 individual wave equations each having its own wave speed and then apply the schemes discussed in Section 3.1. Characteristic decomposition, however, is costly. A simple but effective flux splitting based on the H-CUSP scheme in [5] is given below.

Consider the 1-D Euler equations

$$\frac{\partial w}{\partial t} + \frac{\partial f(w)}{\partial x} = 0 \quad (14)$$

where

$$w = \begin{pmatrix} \rho \\ \rho u \\ \rho E \end{pmatrix} \quad (15)$$

$$f = \begin{pmatrix} \rho u \\ \rho u u + p \\ \rho u I \end{pmatrix} \quad (16)$$

where I is the specific total energy if the absolute reference frame is used. When a rotational reference frame is used as in many turbomachinery codes I is taken to be the rothalpy in the rotational reference frame.

A CUSP scheme splits f into a convective flux f_c and a pressure flux f_p.

$$f_c = u\begin{pmatrix} \rho \\ \rho u \\ \rho I \end{pmatrix} = uw_c \quad (17)$$

$$f_p = \begin{pmatrix} 0 \\ p \\ 0 \end{pmatrix} \quad (18)$$

Dissipation fluxes are then formed separately for f_c and f_p by using the method in Section 3.1. Thus

$$d_{j+\frac{1}{2}} = d_{cj+\frac{1}{2}} + d_{pj+\frac{1}{2}}$$

where for a 1st order scheme

$$d_{cj+\frac{1}{2}} = \frac{1}{2}f_1(M)c_{j+\frac{1}{2}}\Delta w_{cj+\frac{1}{2}}$$

$$d_{pj+\frac{1}{2}} = f_2(M)\begin{pmatrix} 0 \\ \Delta p_{j+\frac{1}{2}} \\ 0 \end{pmatrix}$$

The dissipation coefficients are designed to give appropriate upwinding for both the convective fluxes and the pressure fluxes.

$$f_1(M) = \begin{cases} a_0 + a_2M^2 + a_4M^4 & \text{for } |M| < 1 \\ |M| & \text{for } |M| \geq 1 \end{cases}$$

$$a_2 = \frac{3}{2} - 2a_0$$

$$a_4 = a_0 - \frac{1}{2}$$

where a_0 is used to control the minimum convective diffusion at points where the convective velocity is zero. Normally it is taken as $\frac{1}{4}$.

$$f_2(M) = \begin{cases} \frac{1}{2}M(3-M^2) & \text{for } |M| < 1 \\ sign(M) & \text{for } |M| \geq 1 \end{cases}$$

Notice that a smooth function for $f_2(M)$ is used here instead of the piecewise-continuous function given in [5].

Second order CUSP schemes can be easily formed with the SLIP scheme discussed in Section 3.1. To form a 2nd order CUSP scheme with SLIP, care must be taken in calculating the pressure differences to maintain consistency with other flow variables. This is achieved by forming a left and a right state at each grid interface by interpolating w_c using SLIP limited slopes. Pressures at these two states are then calculated and their difference formed to provide the higher order pressure diffusion term [5].

4 Results and Discussions

The CUSP scheme has been validated on a number of theoretical and practical cases at ABB power generation. Due to its increased accuracy and robustness, the CUSP scheme is now used as the default option in the new code. In this paper, we will first present inviscid results for a simple supersonic wedge cascade and then focus on the performance of the scheme on a three-dimensional turbine vane.

4.1 Supersonic Flow through a Wedge Cascade

Denton [8] proposed a wedge cascade as a test case for capturing oblique shocks with an Euler method. Fig. 1 shows the profiles of the cascade and the Mach number contours calculated by using the baseline code with JST scheme. The inlet Mach number of this cascade is 2. The shock reflected from the lower blade is designed to be exactly cancelled out at the corner of the upper blade, giving a uniform flow between the parallel surfaces and an expansion off the downstream corner. This design gives a good test case for numerical methods for the Euler equations since an exact solution is available analytically. Numerical smearing may prevent complete cancellation of the reflected shock, and thus produce a nonuniform region downstream. This test case is used here to demonstrate the better resolution of shock and expansion waves provided by the new CUSP scheme.

Figure 1, 2, and 3 show the computed Mach number contours, the pressure and Mach number distribution on the blade surface by the baseline code with the JST scheme. Figure 4, 5, and 6 show the corresponding results by using the new CUSP scheme. These figures clearly show sharper and less oscillatory solutions by the new scheme compared to the baseline code across the shock and expansion waves. Of much significance is the Mach number recovery through the expansion fan at the second corner of the blade. Previous calculations, including the one by Denton himself, showed that the largest discrepancy between numerical results and the analytical solution is around the downstream corner where a cluster of expansion waves accelerate the flow to a Mach number a little higher than 2. Large entropy increase is observed behind the expansion waves in the near wall region resulting in a lower Mach number on the blade surface compared to the analytic solution. This can be seen in Figures 1 and 3. Figures 4 and 6 show clearly that the CUSP scheme significantly reduces this error.

Jameson in [5] gave proof for the conditions of a numerical scheme for obtaining single point shock waves. He also presented a variation of the CUSP scheme that satisfies the given conditions. It must be noted that the CUSP scheme implemented in the current studies neglected the $\frac{1}{2}\beta\bar{w}_h\Delta u$ term given in [5] that is needed to satisfy the one-point shock conditions. In addition, such conditions are based on one-dimensional analysis. The above computation does not show a one-point shock structure for the oblique supersonic-to-supersonic shock waves.

4.2 Flow through a Turbine Vane

In this section, we will examine in detail the computation of a turbine vane originally provided in a one and a half stage test case openly available within the framework of the ERCOFTAC workshop[9]. The 3-row configuration was experimentally investigated at the University of Aachen where measurements behind the first vane, the first stage and the full configuration were taken. Emunds, Jennions, Bohn, and Gier presented an exhaustive discussion on the detailed flow mechanism through this 1.5 stage. In this paper, we will restrict ourselves to the vane calculations only. In particular, we will examine the the performance of the CUSP scheme on the prediction of losses on a relatively coarse grid with wall functions.

In most production-mode calculations, relatively coarse grids are used which often do not allow integration of the boundary layer to the wall. Typical y^+ of the first grid point[10] from the wall may range from the tens to the hundreds. Consequently, wall functions are used to obtain the shear stress on the wall instead of by direct calculation based on finite-differencing on the coarse grid. Figure 7 shows such a grid generated for the Aachen vane blade to be used in the current study. The grid con-

sists of $129 \times 37 \times 49$ points. We start with the JST scheme and will focus on the spanwise distribution of the circumferentially-averaged total pressure. The figures shown in the following paragraphs present spanwise distributions of the average total pressure at the inlet to the turbine, a station 8 grid points ahead of the turbine Trailing Edge (TE), and a station 8.8mm downstream of the TE. We will refer to the latter two stations as Station 1 and Station 2, respectively. The inlet stagnation pressure, stagnation temperature, and flow angles are given based on the experiments and are identical to those used by Emunds, Jennions, Bohn and Gier[10]. The experimental data shown in the figures are measured at the station 8.8mm downstream of the turbine TE.

Figure 8 shows the result with the original JST scheme running in Euler mode. Emunds, Jennions, Bohn, and Gier point out that the two total pressure peaks near the hub and casing are due to secondary flow vortices generated in the blade passage with the specified inlet boudary layer profile. Although an Euler calculation does not include the physical viscous effects, it is capable of resolving the passage vortex generation provided the inlet boundary layer is specified and there are sufficient number of grid points to resolve this boundary layer. As shown in Figure 8, the Euler calculation indeed mimics the secondary flow features. The peaks of total pressure are clearly seen in the computed results at both Station 1 and Station 2. In principle, there should be no total pressure loss in an Euler calculation for a subsonic case. We can see that the total pressure level at Station 1 right before the blade trailing edge is very close to that given at the inlet, showing that there is very little numerical contamination of the solution up till this station. The computed total pressure at Station 2 downstream of the trailing edge, however, shows a significant pressure loss which should not exist in an Euler solution. This is due to the fact that we used a blund trailing edge model in the grid. An Euler calculation can not really support such a blunt trailing edge. Numerical dissipation become effective in the trailing edge area, causing the observed total pressure loss at Station 2. Since there is effectively no profile loss, the computed total pressure at Station 2 is still higher than the experimental data.

Figure 9 shows the result with the original JST scheme running full Navier-Stokes for this case. Figure 10 is the convergence history with a 3 level multigrid for this case. Notice that the residual level tends to hang after a reduction of 2-3 orders of magnitude. In order to make the computation further converge, we freeze the turbulence eddy viscosity calculated by the Baldwin-Lomax model at this time. After doing this, it can be seen that the computation continues to converge towards machine zero (only single precision calculation is used in this study). Although the computation has converged, Figure 9 shows that the computed average total pressure deviates very much from the experimental data. In particular, the computed result exhibits large overshoot peaks near the hub and casing. These peaks are non-physical and are due to the fact that the grid is rather coarse. It is well-known that a central-difference type scheme will produce oscilations within a sharp boundary layer where the no-slip boundary condition is applied when the cell Reynolds number is too high. Notice, in this case the switched JST scheme adds no second-order dissipation because there is effectively no pressure gradient within the boundary layer. The overall total pressure levels seem to be even higher than those predicted by the Euler calculations. This is due to the fact that there is also artificial overshoot of total pressure near the blade surfaces, resulting in higher circumferentially averaged total pressures.

To confirm the above argument, we repeated the Navier-Stokes calculations on a fine grid with $129 \times 49 \times 81$ grid points and with more grid clustering near the wall. The result is shown in Figure 11. This time, we see the computational result no longer exhibit the numerical overshoot, and it agrees with the experimental data very well.

The above results show that the original JST scheme with a switched sensor may not be reliable for viscous flows on coarse grids. We now turn our attention to the CUSP scheme. Figure 12 shows the Euler result for the same case with the CUSP scheme. Clearly, the CUSP scheme predicts essentially the same total pressure behavior as the JST scheme for the Euler calculations. Figure 13 shows the result of Navier-Stokes calculations with CUSP. Unlike the JST scheme, the CUSP scheme does not exhibit the artificial total pressure overshoots near the walls. The computed total pressure levels also agree well with the experimental data at Station 2 including the secondary flow features near the end walls. The total pressure at Station 1 is now less than that predicted by the Euler calculations. This is due to the profile loss predicted in the Navier-Stokes code. The difference of total pressure between Station 1 and Station 2 is due to the trailing edge loss which now may be regarded to be more or less physical since the physical viscosity is included and it is significant in that region although it is debatable whether the computation is fully resolving the trailing edge. Because of the coarse grid used near the trailing edge, numerical dissipation may still be significant there which functions to add some numerical total pressure loss. Nevertheless, the compuation does seem to model the physical loss closely with the CUSP scheme on this relatively coarse grid.

Notice that in order to predict the profile loss on a coarse grid where direct integration of the turbulent boundary layer to the wall is not possible,

one has to use a wall function to obtain the correct shear stress on the wall. To confirm this, we run the Navier-Stokes code by turning off the wall function and calculate the wall shear stress directly by differentiating the velocity profiles on the coarse grid. The result is shown in Figure 14. It can be seen that in this case, the total pressure at Station 1 before the blade TE is now almost at the same level as that predicted by the Euler code. Without the wall function, the shear stress is grossly underpredicted on the coarse grid resulting in little profile loss even though the no-slip boundary condition is used.

Figure 15 shows the convergence history of the Navier-Stokes computation for the Aachen vane with the CUSP scheme. It can be seen that the computation exhibits the same level of convergence rate as that for JST scheme. The above results show that the CUSP scheme provides an accurate, reliable method for solving turbulent viscous flows without compromising efficiency, even on coarse grids provided the wall function is used.

5 Concluding remarks

An artificial dissipation scheme based on the concepts of SLIP and CUSP is implemented in a three-dimensional Navier-Stokes code for turbomachinery flow calculations. Comparisons of the computational results by the CUSP scheme with those by the classical JST scalar dissipation scheme show that the CUSP scheme provides better accuracy of shock waves and boundary layers than the JST scheme while retaining the same computational efficiency. The CUSP scheme is capable of providing reasonably good estimate of turbomachinery losses on relatively coarse grid with the use of wall functions while the classical JST scheme tends to give overshoot of total pressure near sharp boundary layers when the grid is not fine enough.

Acknowledgement

Support for this research was provided by ABB Power Generation in Baden Switzerland. The first author also received support from the National Science Foundation under Grant CTS-9410800. The authors are indebted to Drs. Y. Chen, R. Emunds, and J. Yao for their valuable assistance in testing the code.

References

[1] A. Jameson and W. Schmidt and E. Turkel, "Numerical Solution of the Euler Equations by Finite Volume Methods Using Runge-Kutta Time Stepping Schemes", AIAA Paper 81-1259, July, 1981.

[2] ABB Power Generation, Stage3d User Manual, 1997

[3] Liu, F. and Jameson, A., "Multigrid Navier-Stokes Calculations for Three-Dimensional Cascades", AIAA Journal, Vol. 31, No. 10, pp 1785-1791, October, 1993.

[4] Jameson, A., "Analysis and design of numerical schemes for gas dynamics 1, artificial diffusion, upwind biasing, limiters and their effect on accuracy and multigrid convergence" International Journal of Computational Fluid Dynamics, 4:171-218, 1995

[5] Jameson, A., "Analysis and design of numerical schemes for gas dynamics 1, artificial diffusion and discrete shock structure", International Journal of Computational Fluid Dynamics, 4:171-218, 1995

[6] Tatsumi, S., Martinelli, L., and Jameson, A., "Design, Implementation, and Validation of Flux Limited Schemes for the Solution of the Compressible Navier-Stokes Equations", AIAA 94-0647, Jan. 1994.

[7] Tatsumi, S., Martinelli, L., and Jameson, A., "A New High Resolution Scheme for Compressible Viscous Flow with Shocks", AIAA 95-0466, Jan. 1995.

[8] Denton, J. D., " An Improved Time Marching Method for Turbomachinery Flow Calculation," *Journal of Engineering for Gas Turbines and Power*, Vol.105, July 1983.

[9] ERCOFTAC Test Case 6, 1.5 Stage Axial Flow Turbine, ERCOFTAC 1995.

[10] R. Emunds, I. K. Jennions, D. Bohn and J. Gier, "The Computation of Adjacent Blade-Row Effects in a 1.5 Stage Axial Flow Turbine", ASME 97-GT-81, 1997

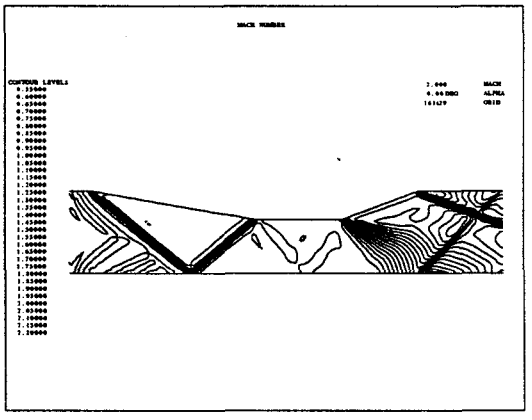

Figure 1: Calculated Mach number contour through a supersonic wedge cascade with JST scheme

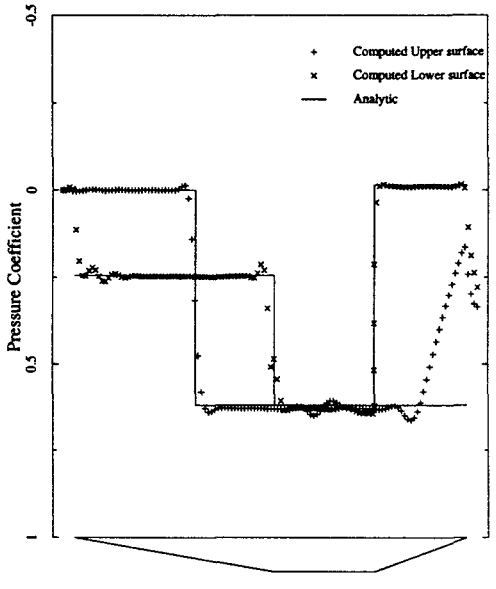

Figure 2: Calculated pressure distribution over a supersonic wedge cascade with JST scheme

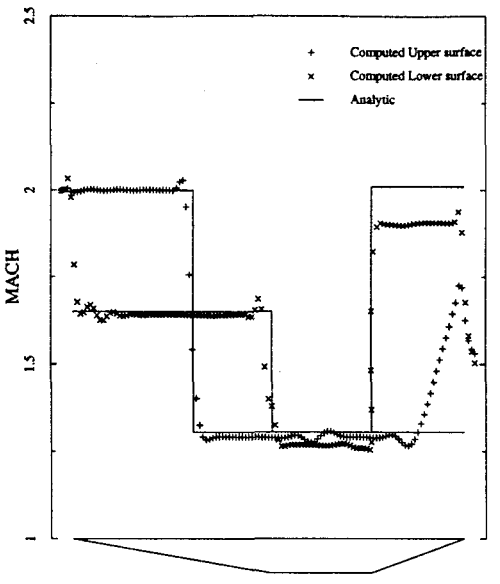

Figure 3: Calculated Mach number distribution over a supersonic wedge cascade with JST scheme

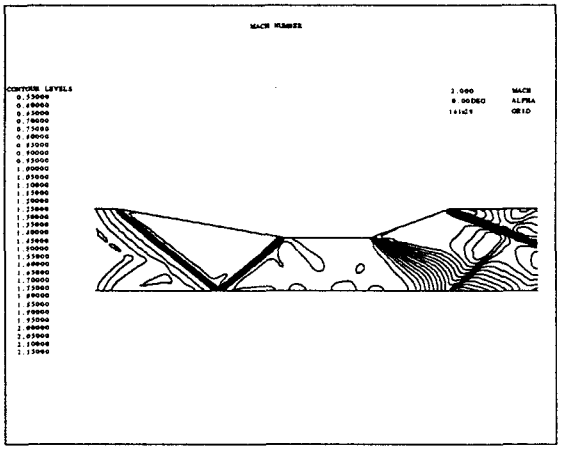

Figure 4: Calculated Mach number contour through a supersonic wedge cascade with CUSP scheme

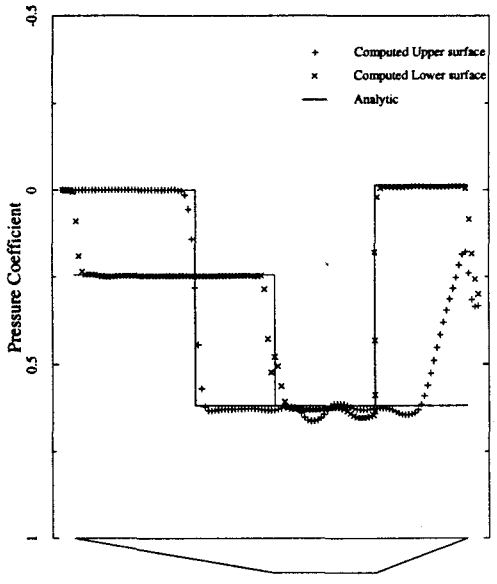

Figure 5: Calculated pressure distribution over a supersonic wedge cascade with CUSP scheme

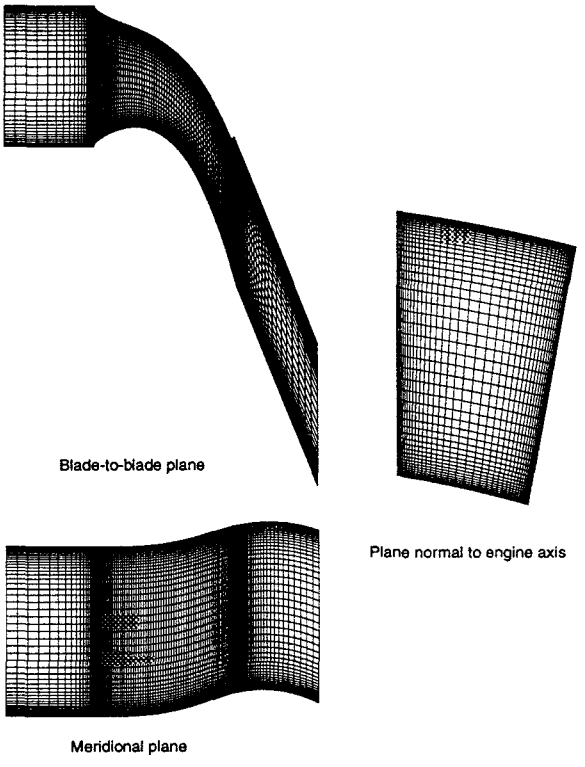

Figure 7: Computational grid for the Aachen vane

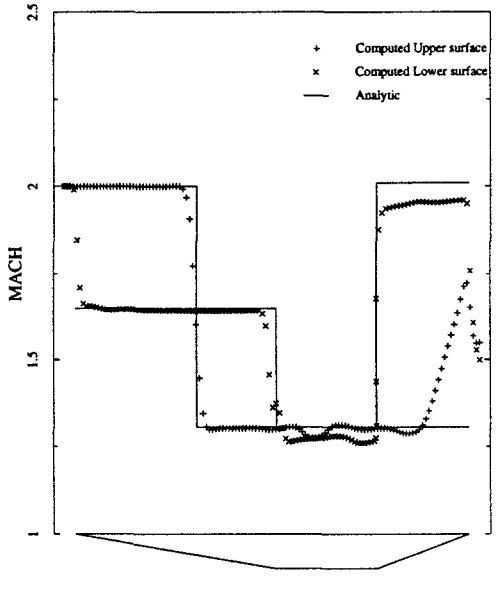

Figure 6: Calculated Mach number distribution over a supersonic wedge cascade with CUSP scheme

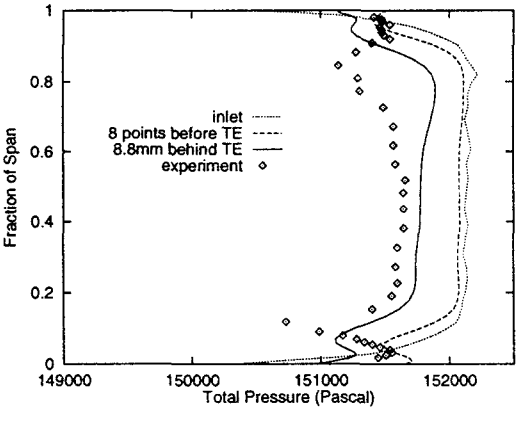

Figure 8: Spanwise distribution of circumferentially averaged total pressure obtained by Euler calculation with JST

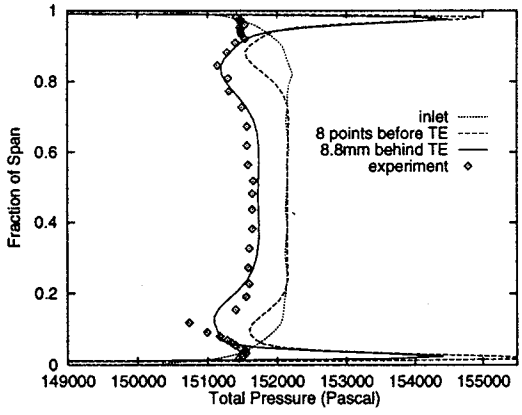

Figure 9: Spanwise distribution of circumferentially averaged total pressure obtained by Navier-Stokes calculation with JST

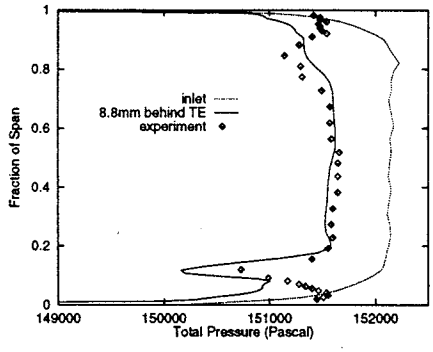

Figure 11: Spanwise distribution of circumferentially averaged total pressure obtained by Navier-Stokes calculation on a fine grid with JST

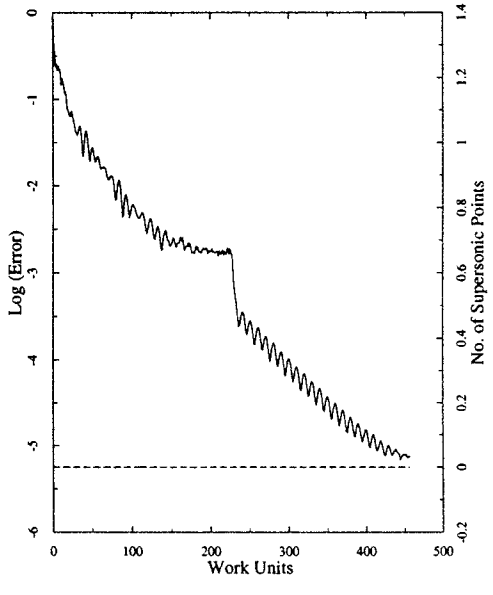

Figure 10: Convergence history for the Navier-Stokes calculation with JST

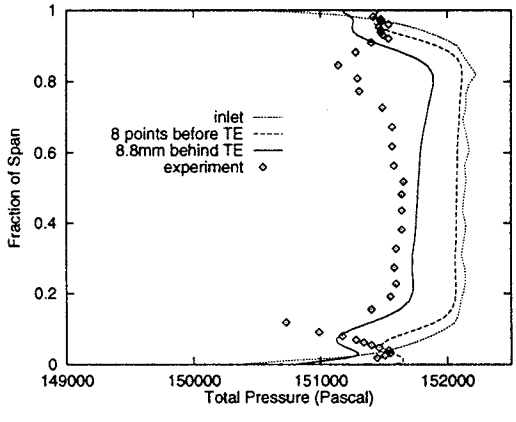

Figure 12: Spanwise distribution of circumferentially averaged total pressure obtained by Euler calculation with CUSP

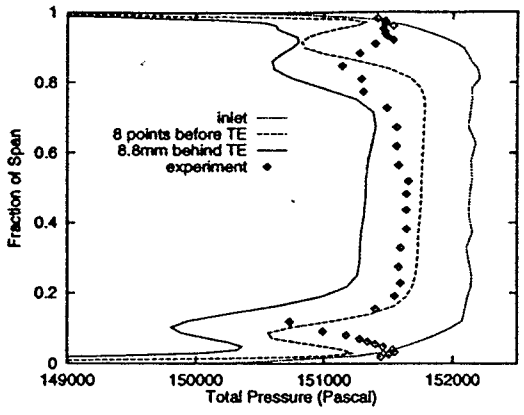

Figure 13: Spanwise distribution of circumferentially averaged total pressure obtained by Navier-Stokes calculation with CUSP and use of wall function

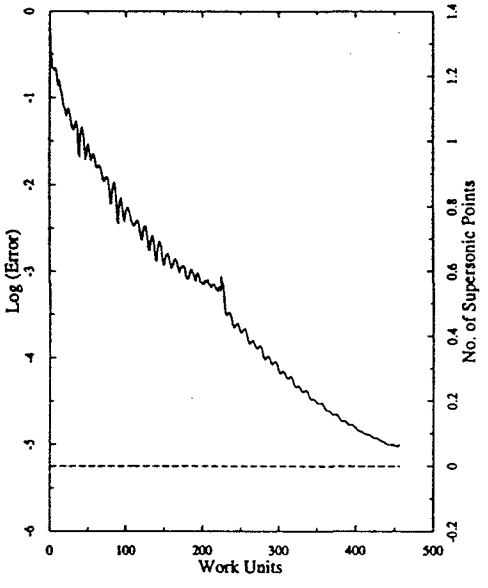

Figure 15: Convergence history for the Navier-Stokes calculation with CUSP

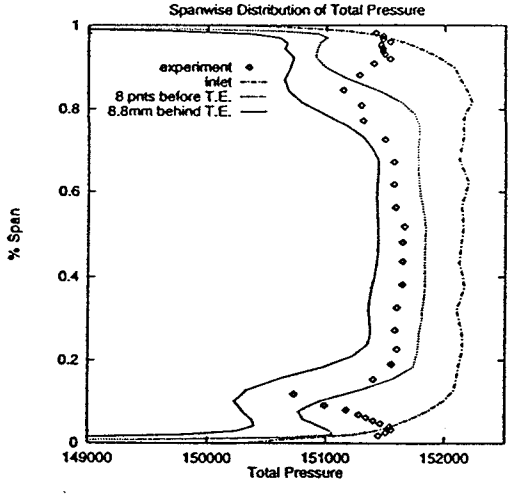

Figure 14: Spanwise distribution of circumferentially averaged total pressure obtained by Navier-Stokes calculation with CUSP and no use of wall function